Supporting Information for "The Relationship Between Cloud Radiative Forcing and Surface Temperature at ENSO Frequencies in CMIP5 Models"

N. J. Lutsko,[1]

Contents of this file

1. Text S1
2. Table S1
3. Figures S1 to S6

Introduction The supplementary material contains one text section, one table and six figures. The text provides more details concerning how the spectra were calculated, as

---

Corresponding author: N. J. Lutsko, Department of Earth, Atmospheric, and Planetary Sciences, Massachusetts Institute of Technology, Cambridge, Massachusetts, USA. (lutsko@mit.edu)

[1]Department of Earth, Atmospheric, and Planetary Sciences, Massachusetts Institute of Technology, Cambridge, Massachusetts, USA.

well as how to interpret the phases and amplitudes. The table lists the name of each model used in the study and the estimates of β_F and ECS from *Forster et al.* [2013] and *Geoffroy et al.* [2013], and the estimates of $\beta_{F,cloud}$ from *Forster et al.* [2013]. The first Figure repeats Figure 2 of the main text, but shows values averaged over the 2.5-5 years^{-1} frequency band. The second Figure shows the results of lag-regressions for each of the models between the low cloud CRE and tropical-mean surface temperatures, between the low cloud CRE and the Nino3.4 index, between the Nino3.4 index and tropical-mean surface temperatures and between the low cloud CRE and tropical-mean cloud cover. The third Figure shows the phase between $\bar{T}'$ and $L(\omega)'$, averaged over frequencies of 2.5 years^{-1} to 3 years^{-1}. The fourth Figure shows scatter plots of the amplitudes for $C(\omega)'$, averaged between 1/3 and 1/2.5 years^{-1} and $\omega = 0$ to 20hPa/day, and the sensitivity estimates for the models. The fifth Figure repeats Figure 4 of the main text, but the regressions are performed between the amplitudes and the estimates of the cloud forcing $\beta_{F,cloud}$ from *Forster et al.* [2013] and the sixth Figure repeats the top panel of Figure 4 of the main text, but the regressions are performed using the amplitudes, averaged over frequencies of 2.5 years^{-1} to 3 years^{-1}, for the regressions between $\bar{T}'$ and $P(\omega)'$.

Text S1. As in *Lutsko and Takahashi* [2018], spectra of the model variables were estimated using Thomson's multitaper method [*Percival and Walden*, 1993], which is similar to the more commonly used periodogram method for estimating spectral density. In the periodogram method, rectangular windows are applied to the data, the power of each filtered signal is calculated and the resulting estimates are then averaged together to produce the final estimate of the spectral density. The multitaper method uses a set of optimal windows (tapers), derived from the discrete prolate spheroid sequences, instead of rectangular windows, producing an improved estimate of the spectral density. The number of windows is a free parameter: using more windows reduces the variance of the estimate, however it also produces more spectral leakage. It was found that using eight windows produced good estimates for the data.

To interpret the phases and amplitudes, note that if $\phi(f) = 0^\circ$ then an increase in $C(\omega)'$ corresponds to an increase in $\bar{T}'$, and the CRE from that bin acts as a negative feedback on surface temperature, while if $\phi(f) = 180^\circ$ then an increase in $C(\omega)'$ corresponds to a decrease in $\bar{T}'$, and the CRE from that bin acts as a positive feedback on surface temperature. In both these cases, $a(\omega)$ can be interpreted as a feedback co-efficient. If $\phi(f) = \pm 90^\circ$ then one variable is proportional to the derivative of the other, with the sign of the relationship ambiguous. For instance, $dC(\omega)'/dt = \bar{T}'$ and $d\bar{T}'/dt = -C(\omega)'$ will both produce a phase of $+90^\circ$. Physical reasoning must be used to differentiate between these two scenarios, with $a(\omega) = f^{-1}$ or f in the two cases, respectively.

If the phase is not equal to 0°, ±90° or 180° then $\bar{T}'$ and C' both have components which are linearly related (and so have a phase of 0° or ±180°) and components which are in quadrature (and so have a phase of ±90°).

References

Forster, P. M., T. Andrews, P. Good, J. M. Gregory, L. S. Jackson, and M. Zelinka (2013), Evaluating adjusted forcing and model spread for historical and future scenarios in the cmip5 generation of climate models, *Journal of Geophysical Research: Atmospheres*, *118*, 1139–1150.

Geoffroy, O., D. Saint-Martin, G. Bellon, A. Voldoire, D. J. L. Olivie, and S. Tyteca (2013), Transient climate response in a two-layer energy-balance model. part ii: Representation of the efficacy of deep-ocean heat uptake and validation for cmip5 aogcms, *Journal of Climate*, *26*(6), 1859–1876.

Lutsko, N. J., and K. Takahashi (2018), What can the internal variability of cmip5 models tell us about their climate sensitivity?, *Journal of Climate*, *31*(13), 5051–5069.

Percival, D. B., and A. T. Walden (1993), *Spectral Analysis for Physical Applications: Multitaper and Conventional Univariate Techniques.*, 1 ed., Cambridge University Press.

Table S1. The models used in this study and their corresponding β_F and ECS estimates from *Forster et al.* [2013] (F13) and *Geoffroy et al.* [2013] (G13). The fourth column shows the $\beta_{F,cloud}$ estimates from *Forster et al.* [2013]

Model	β_F (F13)/(G13) [$\mathrm{Wm^{-2}K^{-1}}$]	ECS (F13)/(G13) [K]	β_{CF} [$\mathrm{Wm^{-2}K^{-1}}$]
BCC-CSM1-1	-1.14/-1.28	2.82/2.9	-0.07
BNU-ESM	n.a./-0.92	n.a./3.9	n.a
CanESM2	-1.04/-1.06	3.69/3.9	0.13
CNRM-CM5	-1.14/-1.12	3.25/3.2	-0.20
CSIRO-Mk3-6-0	0.63/-0.68	4.08/5.1	0.23
FGOALS-s2	-0.92/-0.87	4.17/4.5	-0.48
GFDL-CM3	-0.7/n.a.	3.97/n.a.	0.48
GFDL-ESM2G	-1.29/n.a.	2.39/n.a.	-0.26
GFDL-ESM2M	-1.38/-1.38	2.44/2.5	-0.33
GISS-ESM-LR	-1.79/-2.03	2.11/2.25	-0.48
HADGEM2-ES	-0.64/-0.61	4.59/5.5	0.37
INMCM4	-1.43/-1.56	2.08/1.9	-0.12
IPSL-CM5A-LR	-0.75/-0.79	4.13/4.25	0.7
MIROC5	-1.52/-1.58	2.72/2.8	-0.51
MPI-ESM-LR	-1.13/-1.21	3.63/3.9	-0.04
MRI-CGCM3	-1.25/-1.31	2.60/2.7	-0.09
NCAR-CCSM4	-1.23/-1.4	2.89/3.0	-0.16
NorESM1-M	-1.11/-1.15	2.80/3.25	-0.11

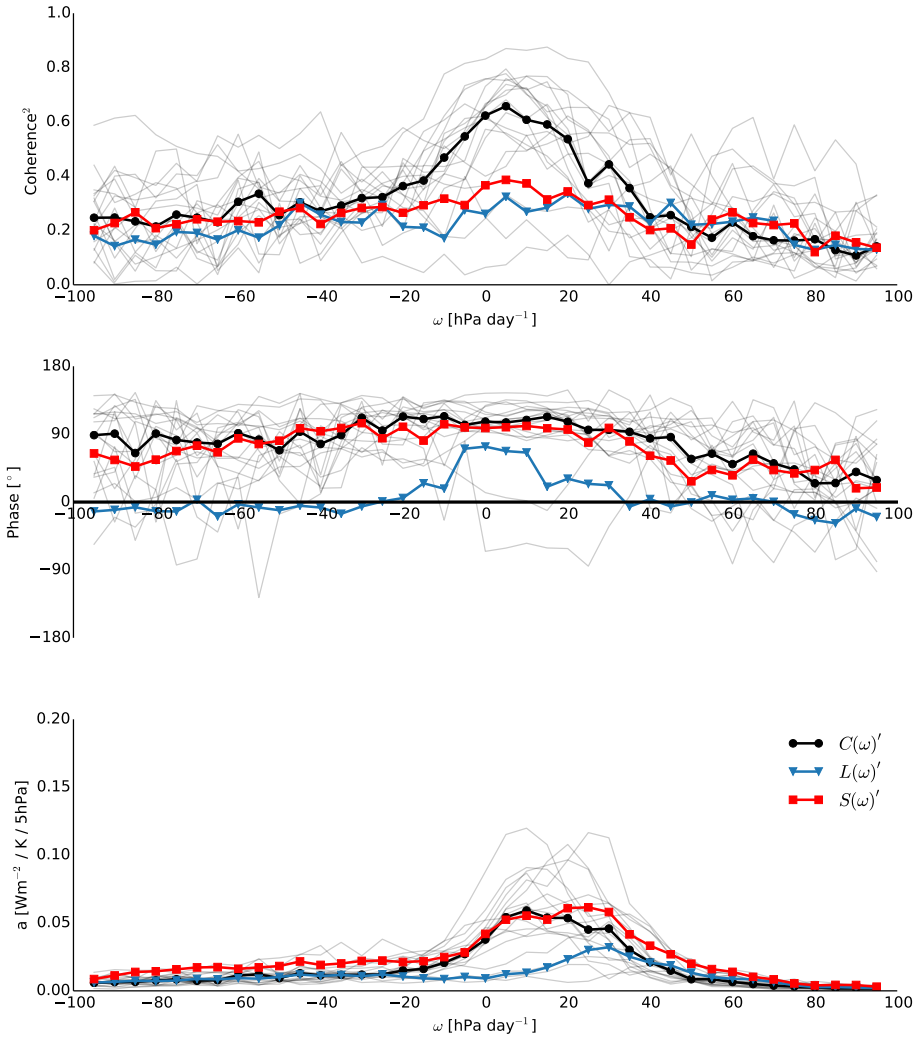

Figure S1. Top panel: squared-coherence between $\bar{T}$ and $C(\omega)'$ for pressure velocities between -100hPaday^{-1} and 100hPaday^{-1}, averaged over frequencies of 2.5 years^{-1} to 5 years^{-1}. The individual models are in gray and the ensemble median is shown by the thick black line. The ensemble-median coherences for the regressions with the long-wave cloud flux ($L(\omega)'$) and the short-wave cloud flux ($S(\omega)'$) are shown in the thick blue and red lines, respectively. Middle panel: same but for the phase between $\bar{T}$ and $C(\omega)'$. Bottom panel: same but the amplitudes between $\bar{T}$ and $C(\omega)'$ are shown.

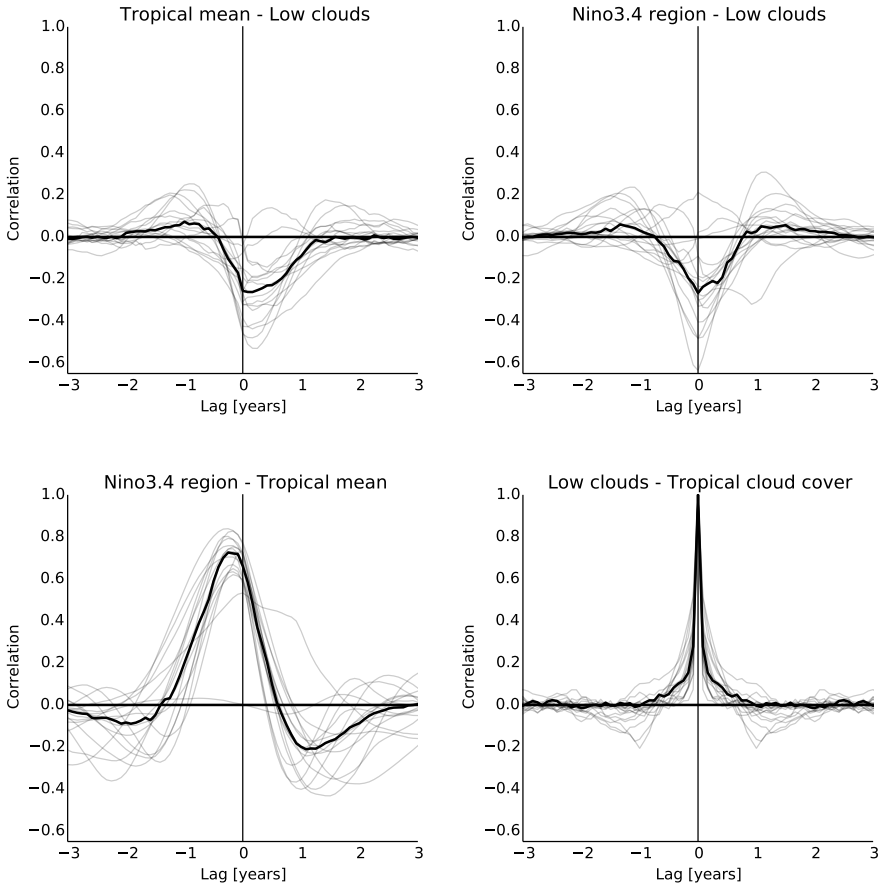

Figure S2. Top left panel: lag correlations between tropical-mean surface temperature and the CRE in subsiding regions (0hPa/day to 40hPa/day). Positive lag means that temperature lags the CRE. The individual models are in gray and the ensemble median is shown by the thick black line. Top right panel: same for the Nino3.4 index and the CRE in subsiding regions. Bottom left panel: same for the Nino3.4 index and tropical-mean temperatures. Positive lag means that the Nino3.4 index lags the tropical mean temperatures. Bottom right panel: same for the CRE in subsiding regions and tropical-mean cloud cover. Positive lag means the cloud cover lags the CRE. The Nino3.4 index was calculated by averaging SSTs in the Nino3.4 box (120°W-170°W and 5°S- 5°N), removing the mean and dividing by the standard deviation, and the lag correlations used de-seasonalized and de-trended monthly data from the models.

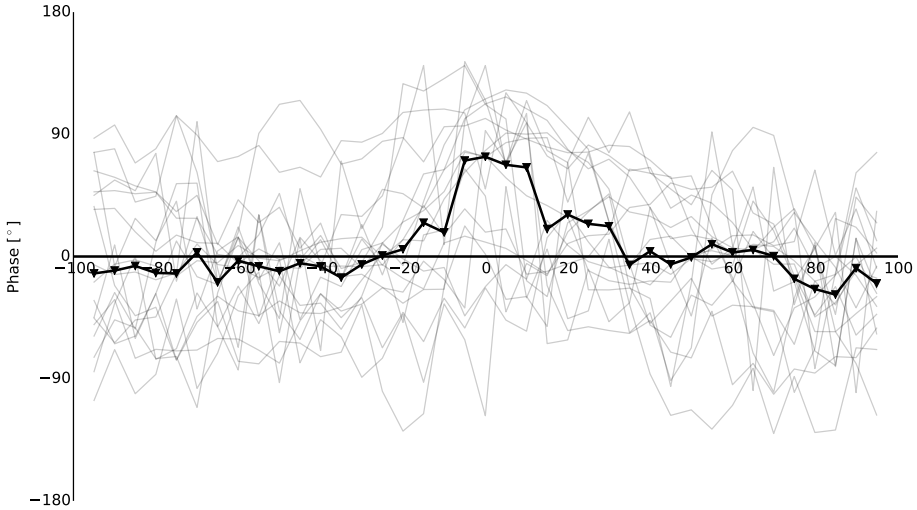

Figure S3. Top panel: phase between $\bar{T}'$ and $L(\omega)'$ for pressure velocities between -100hPaday^{-1} and 100hPaday^{-1}, averaged over frequencies of 2.5 years^{-1} to 3 years^{-1}. The individual models are in gray and the ensemble median is shown by the thick black line.

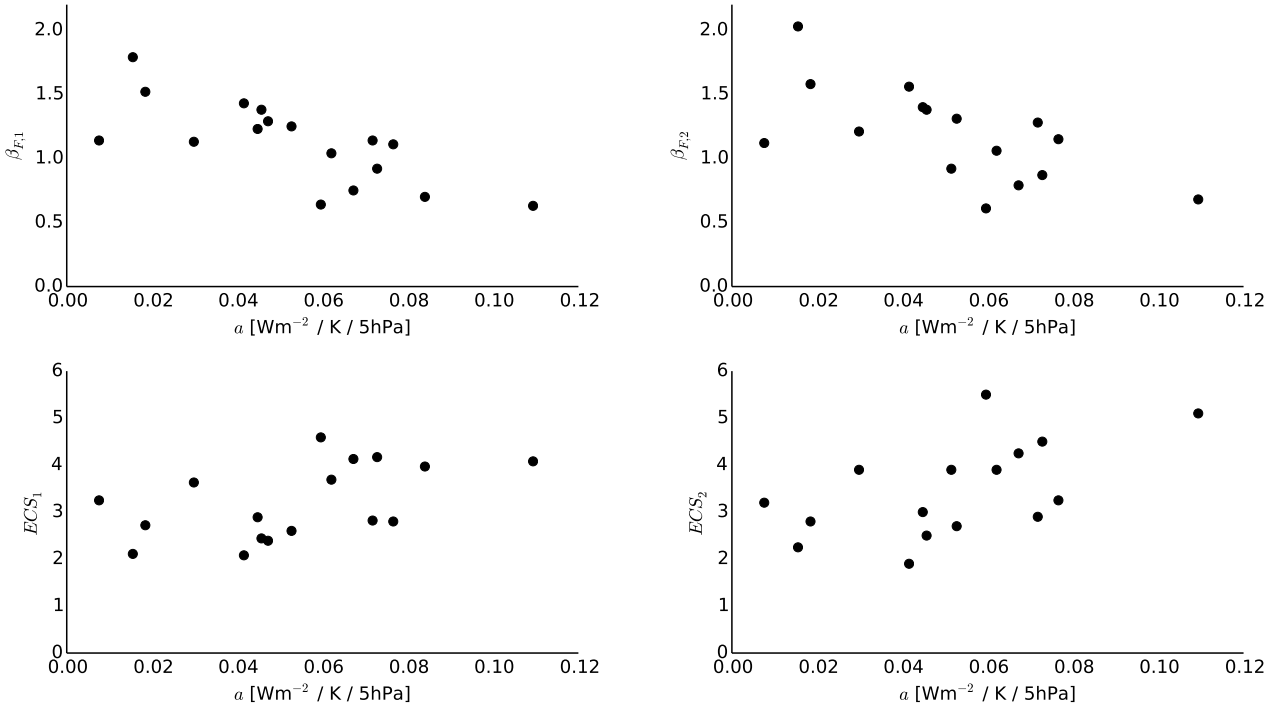

Figure S4. Top left panel: scatter plot of the amplitudes for $C(\omega)'$ averaged between 1/3 and 1/2.5 years^{-1} frequency and $\omega = 0$ to 20hPa/day versus the $\beta_{F,1}$ estimates. Top right panel: same for the $\beta_{F,2}$ estimates. Bottom left panel: same for the ECS_1 estimates. Bottom right panel: same for the ECS_2 estimates.

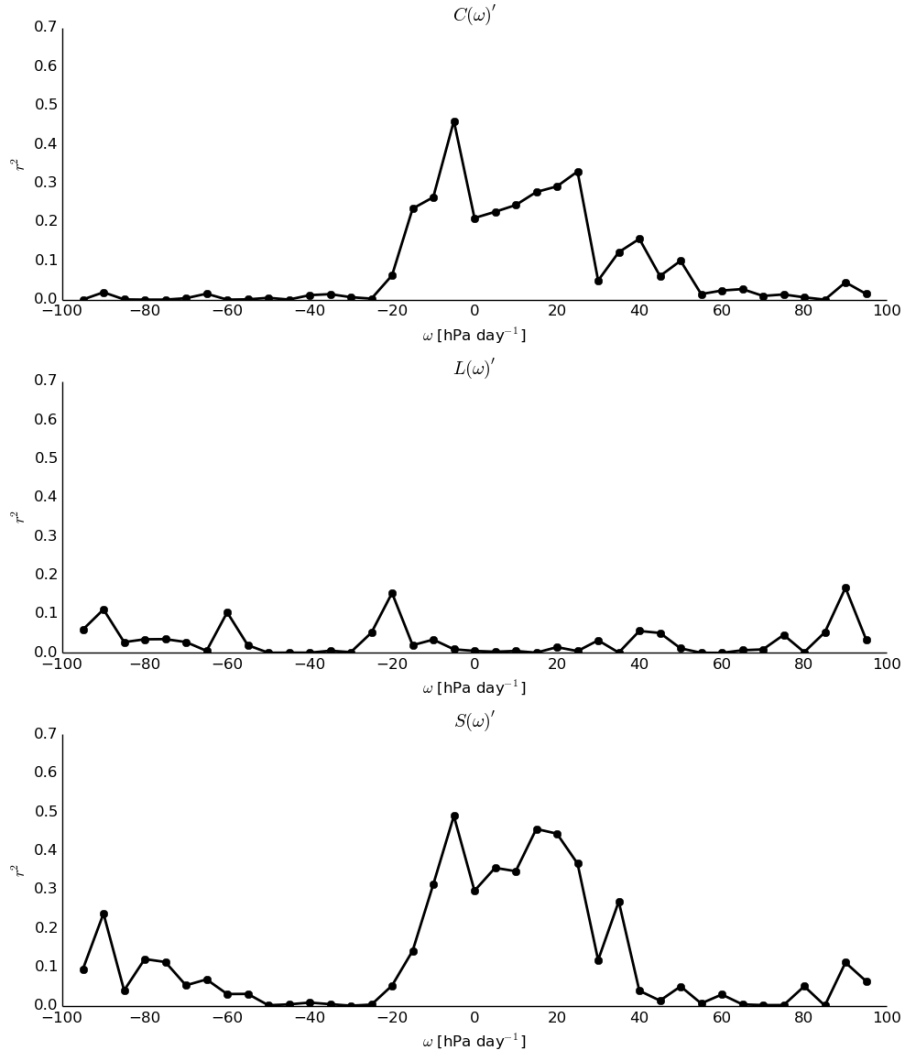

Figure S5. Top panel: r^2 values for regressions between the estimates of $\beta_{F,cloud}$ and the amplitudes, averaged over frequencies of 2.5 years^{-1} to 3 years^{-1}, for the regressions between $\bar{T}'$ and $C(\omega)'$. Middle panel: same for the regressions between $\bar{T}$ and $L(\omega)'$. Bottom panel: same for the regressions between $\bar{T}'$ and $S(\omega)'$.

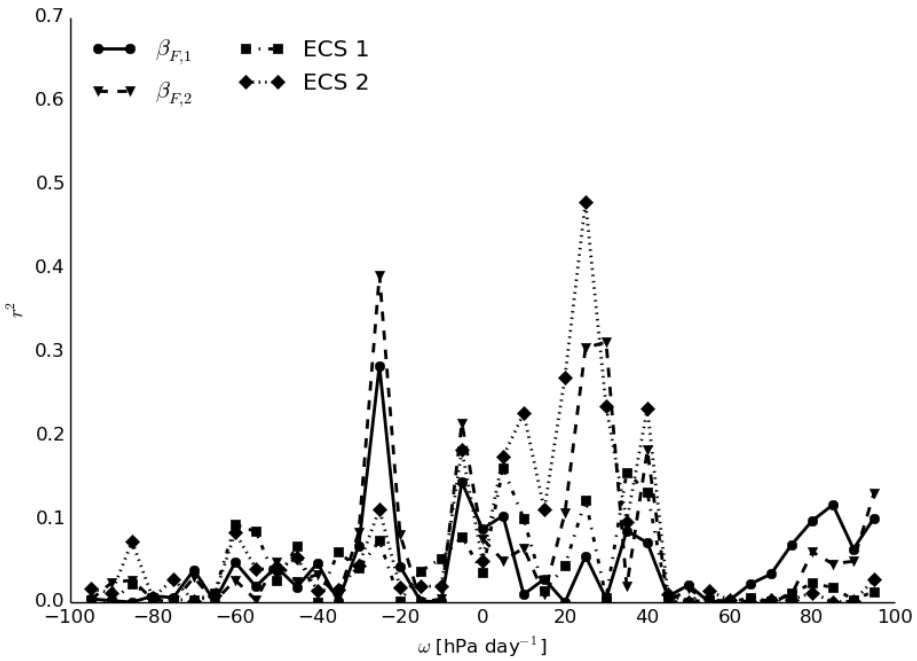

Figure S6. r^2 values for regressions between the four sets of sensitivity estimates and the amplitudes, averaged over frequencies of 2.5 years^{-1} to 3 years^{-1}, for the regressions between $\bar{T}'$ and $P(\omega)'$.